

Xiufang Zhu^{1,2,3}, Dongyan Lu^{3*}, Min Zhao^{4*}, Tingting Liu³, and Shizhe Zhang³

¹Key Laboratory of Environmental Change and Natural Disaster of Ministry of Education, Beijing Normal University, Beijing 100875, China

²State Key Laboratory of Remote Sensing Science, Beijing Normal University, Beijing 100875, China

³Institute of Remote Sensing Science and Engineering, Faculty of Geographic Sciences, Beijing Normal University, Beijing 100875, China

⁴Center for Geodata and Analysis, Faculty of Geographical Science, Beijing Normal University, Beijing 100875, China

Corresponding author: Dongyan Lu (202221051098@mail.bnu.edu.cn); Min Zhao (zhaomin@bnu.edu.cn)

Key Points:

- The drought hazard index (DHI) was constructed by synthesizing drought frequency, duration, intensity and peak
- DHI and its change were estimated under 2 °C, 3 °C and 4 °C temperature rise scenarios based on 18 climate models of CMIP6
- The national average increase values of DHI at 3 °C and 4 °C temperature rise are 1.5 times and 2 times that at 2 °C temperature rise

Abstract

Drought is one of the most disastrous extreme climate events. In-depth studies on the response of drought to climate warming are beneficial to improve drought risk management. In this study, the standardized precipitation evapotranspiration index (SPEI) was calculated based on eighteen climate models from the Coupled Model Intercomparison Project Phase 6 (CMIP6). Four drought characteristic indices (drought frequency, duration, intensity, and peak) were extracted and the drought hazard index (DHI) was constructed to evaluate drought hazards in China for the historical reference period and future 2, 3 and 4 °C temperature rise scenarios, and then the change in future drought hazard was analyzed. The results showed that the drought frequency in the eastern monsoon region of China had a spatial pattern of high in the south and low in the north and increased overall with the increase in warming level. Drought duration, intensity and peak showed a spatial pattern of high in northwest China and low in southeast China and increased significantly with increasing warming level. The DHI was relatively high in the northwest inland and southeast coast of China. Under the 2, 3 and 4 °C temperature increase scenarios in the future, except for the southeastern Qinghai-Tibet Plateau, the DHI in other climate regions in China will increase compared with that in the historical reference period. The national average increase values of DHI under the 3 °C and

4 °C temperature rise scenarios reach 1.5 times and 2 times that under the 2 °C temperature rise scenario, respectively.

Plain Language Summary

Drought is one of the most widespread natural hazards and has caused serious economic losses. Global warming has contributed to increasing drought frequency and intensity in some areas in recent years, and therefore it is necessary to study the response of drought hazards to different global warming levels. In this study, the characteristics of drought events in China were extracted for the historical reference period (1985-2014) and future 2 °C, 3 °C and 4 °C temperature rise scenarios based on the climate simulation data. The drought hazard index (DHI) was constructed by integrating four drought characteristic indices and the change in DHI was estimated at different warming levels. We find that the drought characteristics and DHI have obvious spatial differentiation and their values in most of China increase with increasing warming level. The DHI values under 2 °C, 3 °C and 4 °C temperature rise scenarios increase relative to that during the historical reference period in China except for the southeastern Qinghai-Tibet Plateau. The results of this study can provide a scientific basis for drought prevention and response in the context of global warming.

Keywords: Drought; hazard; temperature rise scenario; CMIP6; China

1 Introduction

Drought is one of the most extensive natural disasters in a series of extreme climate events and has an impact on the water resource supply, agricultural production, ecology, energy, economy, and many other aspects (Chen et al., 2021). According to the Sixth Assessment Report (AR6) of the Intergovernmental Panel on Climate Change (IPCC), the magnitude of natural disaster risk in the context of climate change depends on the interactions between climate-related hazards and the exposure and vulnerability of human or ecological systems to hazards (IPCC, 2022a). Hazard is a necessary condition in the formation of disasters (Shi et al., 2020). Therefore, an accurate understanding and assessment of drought hazards is the premise and foundation of drought risk analysis.

Drought characteristics such as frequency, duration, and intensity are manifestations of drought hazards (Hayes et al., 2004). Some researchers identified drought events based on the drought index and extracted drought characteristics to quantitatively describe drought events to carry out drought hazard analysis (Liu et al., 2021; Nam et al., 2015; Yuan et al., 2013). Researchers constructed a drought hazard index by combining multiple drought characteristics to indicate the drought hazard level (Geng et al., 2016; He et al., 2011; Maccioni et al., 2015). Due to the complexity of drought and regional differences, there is no unified method to calculate the drought hazard index. However, both the extraction of drought events and the construction of drought hazard indices are often

based on various drought indices. The Handbook of Drought Indicators and Indices released by the World Meteorological Organization (WMO) and the Global Water Partnership (GWP) lists 50 commonly used drought indicators/indices, which are grouped into five types: meteorology, soil moisture, hydrology, remote sensing and composite/modeled (WMO & GWP, 2016). Among them, the most commonly used drought indices include the Palmer drought severity index (PDSI) (Palmer, 1965), standardized precipitation index (SPI) (McKee et al., 1993) and standardized precipitation evapotranspiration index (SPEI) (Vicente-Serrano et al., 2010). The PDSI is established based on the principle of soil water balance. It comprehensively considers factors such as precipitation, potential evapotranspiration, runoff, and soil water. The physical meaning of the PDSI is clear, but it has problems such as a single time scale and complex calculations (Yihdego et al., 2019). The definition and calculation of the SPI is relatively simple. It only takes precipitation as the input and does not consider the influence of temperature. Therefore, it has certain limitations in drought research under the background of global warming (Mukherjee et al., 2018). The SPEI improves the SPI and adopts the difference between precipitation and evapotranspiration. It not only has the advantages of simple calculation and multiple time scales, but also considers the sensitivity of evapotranspiration to temperature change (Yihdego et al., 2019). The SPEI has been widely used in drought-related research (Ayantobo et al., 2018; Li et al., 2021; Spinoni et al., 2020).

Global warming has become a major environmental problem in the 21st century, and its negative effects seriously threaten the development of human society. According to IPCC AR6, the global average temperature from 2001 to 2020 increased by approximately 0.99 °C compared with preindustrial levels (IPCC, 2021). With global warming, extreme climate events such as heat waves, heavy rainfall and drought have intensified in recent years, causing serious losses to society, the economy and people’s lives (Zhang & Wang, 2019). To mitigate the serious threat posed by climate change, the Paris Agreement adopted at the 2015 Paris Climate Conference pointed out that the global average temperature in this century should be controlled within 2 °C higher than that of the preindustrial period, and efforts should be made to control the increase within 1.5 °C (Rogelj et al., 2016). In this context, the projection of climate change and its impacts under different temperature rise scenarios in the future has attracted increasing attention from researchers.

Many researchers use general circulation models (GCMs) to assess or predict the risk of future extreme climate. GCMs are approximate representations of the real climate system. The Coupled Model Intercomparison Project (CMIP) organized by the World Climate Research Programme (WCRP) publicly provides many GCM outputs in a standard format. To date, the CMIP has evolved into its sixth phase (CMIP6), providing strong data support for research in the field of climate change (Eyring et al., 2016). Some studies have pointed out that compared with CMIP5, CMIP6 has improved the simulation of extreme events (Chen et al., 2020; Fan et al., 2020; Luo et al., 2020). Therefore, some

researchers have analyzed the characteristics and changes in extreme climate in different regions of the world in the future based on CMIP6, such as extreme precipitation (Dike et al., 2022; Tang et al., 2021; Wu et al., 2022; Xu et al., 2022), extreme temperature (Babaousmail et al., 2022; Kuang et al., 2021; Rajulapati et al., 2022; Zhao et al., 2021), heat waves (Zachariah et al., 2021) and drought (Chen et al., 2021; Cook et al., 2020; Naderi et al., 2022; L. Zhang et al., 2021).

Drought occurs frequently in China, and drought-related economic losses account for approximately 35% of all losses caused by natural disasters in the country (Li et al., 2020). From 1984 to 2018, the average annual direct economic loss caused by drought in China exceeded 34 billion yuan (Su et al., 2021). Affected by global warming, in recent years, some areas of China have shown a trend of expanding drought area and increasing drought intensity (Yu et al., 2014). Some studies based on GCMs also point out that China is a hot area affected by drought (Cook et al., 2020; Ukkola et al., 2020). The impact of drought on Chinese people’s lives and social economy may continue to increase in the future. Currently, some researchers have assessed future droughts in China based on CMIP6 climate data. For example, Chen et al. (2021) projected drought conditions in China using the self-calibrated Palmer drought severity index (scPDSI) based on 20 GCM simulations from CMIP6 and analyzed the socioeconomic impacts of drought. G. Zhang et al. (2021) assessed the performance of standardized moisture anomaly index (SZI), SPEI, and scPDSI in identifying drought across China based on simulations from CMIP6 GCMs and determined drought characteristics based on SZI from 1985 to 2100. Su et al. (2021) and Ma et al. (2022) calculated the SPEI of historical and future periods and then evaluated the spatiotemporal characteristics of drought across China. The above studies all analyzed the changes in drought characteristics (such as drought frequency, drought duration, drought intensity, etc.) in a certain period of time in the future, but few researchers construct hazard indices from the perspective of drought risk. In addition, research on future drought is mostly based on different CMIP6 climate scenarios. There is little assessment of drought under different temperature rise scenarios (such as 2 °C, 3 °C and 4 °C). Global or regional climate change under different temperature rise scenarios has been widely studied by the international scientific community. The assessment of China’s drought under different temperature rise scenarios can provide a decision-making basis for the formulation of regional disaster reduction programs and measures and is very important to improve the drought disaster risk management level and the ability of forecasting and early warning.

The global temperature rise level can be estimated by calculating the increase in global mean surface air temperature (GSAT) averaged over a 30-year period relative to the preindustrial level, and the reference period 1850-1900 was used to approximate the preindustrial GSAT (IPCC, 2021, 2022b). The Fifth Assessment Report (AR5) of the IPCC (2014) takes 1986-2005 as the baseline period and puts forward that the average temperature in this period is approximately 0.61 °C higher than preindustrial levels. Therefore, 0.89 °C higher than the av-

erage temperature in the baseline period 1986-2005 is defined as a temperature rise level of 1.5 °C. Similarly, a higher warming level can be calculated. However, the latest IPCC AR6 revised the temperature rise level in the baseline period of AR5 from 0.61 °C to 0.69 °C and updated the baseline period to 1995-2014, which was 0.85 °C warmer than the preindustrial level (IPCC, 2021). To date, a large number of studies have used the baseline period with the underestimated warming of 0.61°C proposed by IPCC AR5 (Jiao & Yuan, 2019; Liu et al., 2020; Miao et al., 2020; Su et al., 2018), and few researchers have conducted climate change research under different temperature rise scenarios based on the newly updated baseline period.

In summary, based on the CMIP6 multimodel outputs, this study selected 1995-2014 as the baseline period to determine the 2 °C, 3 °C and 4 °C temperature rise scenarios and calculated the SPEI to reflect meteorological drought. On this basis, drought characteristics (drought frequency, duration, intensity, and peak) were extracted for both the historical reference period and different temperature rise level scenarios. Finally, the drought hazard index was constructed, and the spatial distribution maps of the drought hazard index in four periods, including the historical reference period and the future 2 °C, 3 °C and 4 °C temperature rise scenarios, were made and compared. The research results can provide a scientific reference for the formulation of drought adaptation measures in China under the background of climate change, as well as provide a reference for drought hazard assessment in other regions.

2 Study Area and Data

2.1 Study Area

China is a vast country with complex terrain. Located in the eastern part of Asia, China has a typical monsoon climate. According to natural conditions such as topography and climate, mainland China is divided into seven climate regions (Zhao, 1983) (Figure 1), including the Northeast humid/semihumid temperate region (Region A), North China humid/semihumid warm-temperate region (Region B), Central and Southern China humid subtropical region (Region C), South China humid tropical region (Region D), Inner Mongolia steppe region (Region E), Northwest desert areas (Region F) and Qinghai-Tibet Plateau (Region G). This regionalization scheme has many applications in drought-related research (Ayantobo et al., 2018; Yao et al., 2018; G. Zhang et al., 2021), so we use it in this study to compare the spatial distribution and changes in drought hazards in different regions.

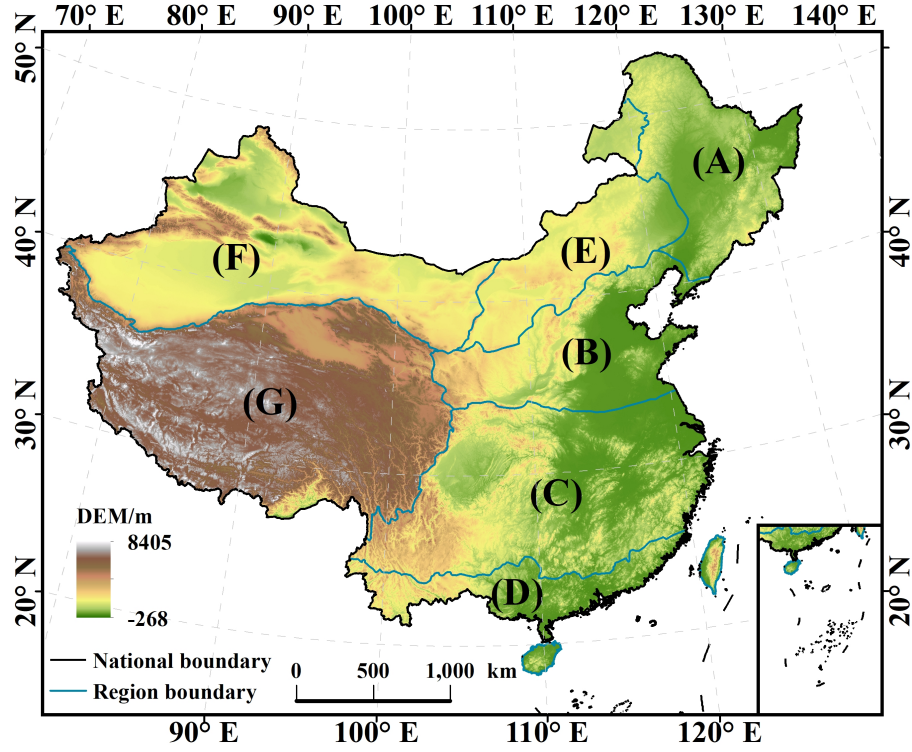


Figure 1. Seven climate regions of China, i.e., Northeast humid/semihumid temperate region (A), North China humid/semihumid warm-temperate region (B), Central and Southern China humid subtropical region (C), South China humid tropical region (D), Inner Mongolia steppe region (E), Northwest desert areas (F) and Qinghai-Tibet Plateau (G).

2.2 Data

(1) Climate observation data

The observational dataset used in this study was the gridded dataset CN05.1 with a spatial resolution of 0.25° , which was interpolated based on the observations from over 2400 stations from 1961 to the present in China (Wu & Gao, 2013). The meteorological variables used in this research include maximum temperature, minimum temperature, precipitation, wind speed, relative humidity and sunshine hours on a monthly scale from 1961 to 2014. This dataset was used as reference data to evaluate the CMIP6 historical simulation data.

(2) CMIP6 climate model datasets

CMIP6 historical simulation data and future projection data were obtained from the World Climate Research Programme (WCRP) (<https://esgf-node.llnl.gov/projects/cmip6/>). Climate projection data are provided for eight integrated

scenarios that combine shared socioeconomic pathways (SSPs) and radiative forcing pathways (O'Neill et al., 2016). We selected three climate scenarios, namely, SSP1-2.6 (low societal vulnerability and low forcing level), SSP2-4.5 (intermediate societal vulnerability and intermediate forcing level) and SSP5-8.5 (high societal vulnerability and high forcing level). In this study, monthly scale data of eight meteorological variables, including mean temperature, maximum temperature, minimum temperature, precipitation, wind speed, relative humidity, downwelling shortwave radiation, and surface air pressure, were downloaded for the historical period (1961-2014) and the future period (2015-2100). At the time of writing (May 2022), considering the availability of the required meteorological variables and securing the variant level “r1i1p1f1”, 18 eligible GCMs were screened, and the information of these models is shown in Table 1.

(3) Elevation data

The Global Multiresolution Terrain Elevation Data 2010 (GMTED2010) dataset was provided by the United States Geological Survey (USGS) (Danielson & Gesch, 2011). In this study, the 30-arc-second (1 kilometer) GMTED2010 data were used to calculate the SPEI based on the FAO-56 Penman Monteith equation.

Table 1. Eighteen CMIP6 GCMs adopted in this study.

No	Model	Institution	Country	Resolution (Lon/°×Lat/°)
	ACCESS-CM2	CSIRO-ARCCSS	Australia	×1.25
	ACCESS-ESM1-5	CSIRO	Australis	×1.24
	CanESM5	CCCma	Australis	×2.81
	CAS-ESM2-0	CAS	China	×1.41
	CMCC-ESM2	CMCC	Italian	×0.94
	EC-Earth3	EC-Earth-Consortium	Europe	×0.70
	EC-Earth3-Veg	EC-Earth-Consortium	Europe	×0.70
	EC-Earth3-Veg-LR	EC-Earth-Consortium	Europe	×1.13
	FGOALS-g3	CAS	China	×2.25
	FIO-ESM-2-0	FIO-QLNM	China	×0.94
	GFDL-ESM4	NOAA-GFDL	USA	×1.00
	INM-CM4-8	INM	Russia	×1.50
	INM-CM5-0	INM	Russia	×1.50

No	Model	Institution	Country	Resolution (Lon/°×Lat/°)
	IPSL-CM6A-LR	IPSL	France	×1.26
	MIROC6	MIROC	Japan	×1.41
	MPI-ESM1-2-HR	DKRZ	Germany	×0.94
	MPI-ESM1-2-LR	MPI-M	Germany	×1.88
	MRI-ESM2-0	MRI	Japan	×1.13

3 Methods

3.1 Simulation Performance Assessment of CMIP GCMs

The Taylor diagram provides a statistical summary of how closely model-simulated patterns match observations by displaying the correlation coefficient (R), the standard deviation (SD), and root mean square error (RMSE) (Taylor, 2001) on a 2-D graph. To evaluate the performance of the 18 GCMs, we used the standardized Taylor diagram in which the SD and RMSE values of the observations and simulations were divided by the standard deviation of the observations to eliminate dimensional effects (Ma et al., 2022; Zhang et al., 2020). A large R value indicated a high correlation between the simulated and observational data. The closer the SD was to 1, the closer the standard deviation between simulated and observational data. The closer RSME was to 0, the smaller the deviation of the simulated data from the observational value.

3.2 Warming Level Estimation

The projections of future global warming were normally made by adding projected warming above a recent past baseline to the observed warming above preindustrial level, and the recent past baseline period was updated from 1986-2005 to 1995-2014 with the observed warming of 0.85 °C according to IPCC AR6 (IPCC, 2021). Therefore, the 2, 3, and 4 °C warming levels were translated to 1.15, 2.15, and 3.15 °C above the 1995-2014 mean in this study. Based on the monthly gridded temperature data, the annual global mean surface air temperature (GSAT) was calculated using the area-weighted average method. By applying the time sampling approach (James et al., 2017), a 30-year moving window was used to calculate the 30-year average GSAT from 2015 to 2100, and the 2, 3, and 4 °C warming periods were defined as the 30-year period when the specific warming levels were first reached for each model under the three integrated scenarios.

3.3 SPEI Calculation and Drought Characterization

The standardized precipitation evapotranspiration index (SPEI) was used for drought event identification. The SPEI is relatively simple to calculate and considers the impact of temperature on drought (Ma et al., 2022). It was constructed by the difference between monthly precipitation and potential evapotranspiration (PET), and then the difference was fitted to the three-parameter log-logistic distribution, which was further transformed to a normal distribution (Vicente-Serrano et al., 2010). The PET was estimated using the FAO-56 Penman Monteith method based on the “penman” function in the R package “SPEI” (Beguería et al., 2014). The SPEI was calculated for a 1-month time scale at each grid to reflect meteorological drought. For each GCM, the distribution function parameters were first computed in the historical period (1961–2014) and were then utilized for the calculation of the SPEI in the future period (2015–2100) under three integrated scenarios, which makes the values in the future period comparable with those in the historical period (Li et al., 2021; Su et al., 2021; Touma et al., 2015).

Run theory is a common method to extract drought characteristic variables, which identifies the beginning and end of drought events by judging the relationship between the drought index and the threshold (Yevjevich, 1967). The traditional run theory uses a single threshold, which may reduce the accuracy of drought event identification (Wang et al., 2020). In this study, three thresholds ($R_0 = 0$, $R_1 = -0.5$, and $R_2 = -1$) were set according to a previous study (Ma et al., 2022). Each drought event was characterized by three variables, namely, duration, intensity and peak. Drought duration was the number of months of a drought event from its occurrence to termination. Drought intensity and peak were the absolute values of the mean and minimum SPEI values during the drought event, respectively. The drought event series at each grid were identified as follows:

- (1) When the value of the monthly SPEI fell below R_1 , we defined that drought occurred in this month.
- (2) When the preliminarily identified drought event lasting only one month showed a higher SPEI value than R_2 , this event was removed.
- (3) Two adjacent drought events were merged into one drought event if they were separated for only one month and the SPEI value of the month was less than R_0 .

In this study, the drought duration, intensity and peak were calculated by averaging the corresponding variables for all individual drought events at each grid in the historical reference period (1985–2014) and 2, 3, and 4 °C warming periods. Drought frequency was defined as the number of drought events that occurred per year, which was obtained by dividing the number of drought events in a 30-year period by 30.

3.4 Drought Hazard Assessment and Change Analysis

For each 30-year period, we obtained the spatial distribution maps of four drought characteristics, namely, drought frequency (F), drought duration (D), drought intensity (I) and drought peak (P). The four drought characteristics reflected the drought from different aspects, but they were not conducive to the comprehensive and intuitive description of the drought hazard. Therefore, the drought hazard index (DHI) was constructed based on the four drought characteristics (Singh et al., 2019):

where W_1 , W_2 and W_3 are weight coefficients, all taken as 1/3; $(FD)'$, $(FI)'$ and $(FP)'$ are the normalized values of the product indicators obtained by multiplying drought frequency (F) by drought duration (D), drought intensity (I) and drought peak (P), respectively.

Drought duration, intensity and peak describe the magnitude of each drought event on average, but the drought hazard in a certain period also depends on the number of drought occurrences. Therefore, the three product indicators obtained by multiplying the three drought characteristics (D, I and P) with the drought frequency (F) can characterize the drought condition per unit of time. The normalization of the three product indicators was performed by the maximum-minimum method. To make the values of different warming periods comparable with those of the historical reference period, the maximum and minimum used for normalization were found in all values of the historical reference period and warming periods at the grids in China. After processing, DHI maps were made for different GCMs.

Finally, the spatial resolution of the distribution maps of the four drought characteristics and the DHI calculated from different GCMs was resampled to $0.5^\circ \times 0.5^\circ$ using the bilinear interpolation method to facilitate the calculation of the mean values of the corresponding data for the historical reference period and 2, 3, and 4 °C warming scenarios (subsequently referred to as the four periods) so as to obtain the final spatial distribution maps of the four drought characteristics and the DHI for the four periods. The DHI was divided into eight levels using the quantile method to characterize different levels of drought hazard. The DHI under the future warming scenario was compared with that of the historical reference period to analyze the change in drought hazard.

4 Results and Analysis

4.1 Performance Evaluation of CMIP6 GCMs

As the SPEI was calculated using the difference between precipitation and PET, the capability of GCMs to describe drought depends on their ability to simulate precipitation and PET. Based on the observational and simulated values of precipitation and PET during the historical period (1961-2014), the performance of 18 GCMs was evaluated using the standardized Taylor diagram method (Fig-

ure 2). The correlation coefficients between simulated data and observational data ranged from 0.52 to 0.71 for precipitation, while they ranged from 0.88 to 0.93 for PET. The ratio of the standard deviation of precipitation between simulations and observations was greater than 1 for each model, and the maximum value was 1.61, while the SD values of PET ranged from 0.94~1.39, most of which were close to 1. The RMSE values for precipitation and PET ranged from 0.77~1.26 and 0.37~0.69, respectively. Although the simulation of precipitation was not as effective as that of PET, the simulated data had generally satisfactory performance for both precipitation and PET and were qualified to be used to assess historical and future drought hazards in China.

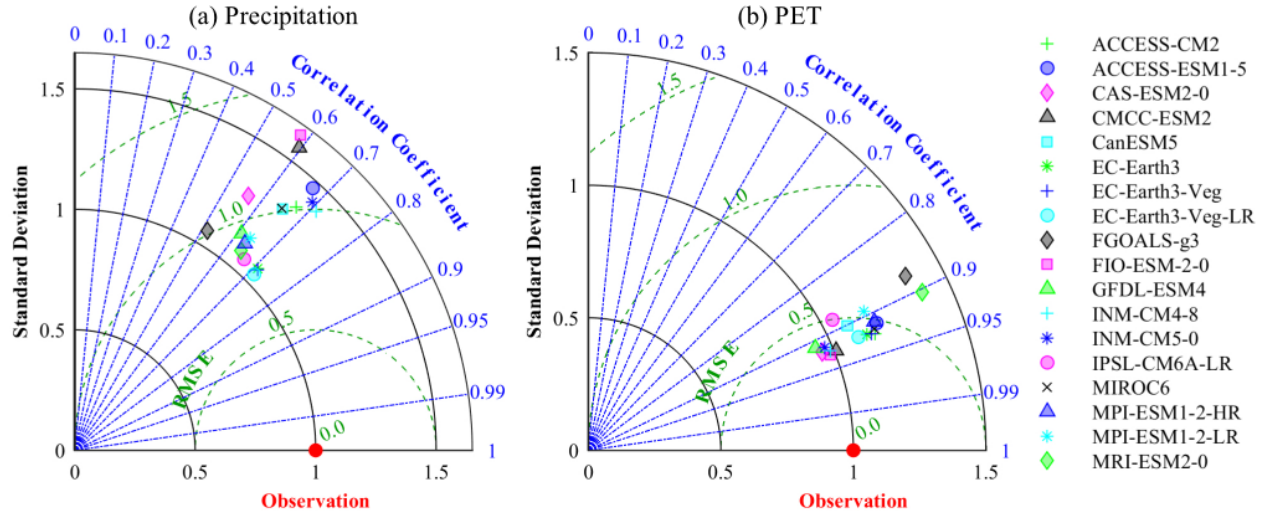


Figure 2. Standardized Taylor diagrams showing the simulation capability of historical simulation data of 18 GCMs from 1961-2014 for observational data of precipitation (a) and PET (b).

4.2 Results of Future Temperature Rise Scenario Determination

The 2, 3, and 4 °C warming periods of 18 models under 3 integrated scenarios were counted, and the 15th year of the 30-year period is presented in Figure 3 as the warming target year. Since SSP1-2.6 was a low emission forcing scenario with a relatively small temperature rise, only 9 models reached the 2 °C warming level in this scenario, and the earliest warming target year was 2034, while the latest was 2081. All models failed to reach the 3 and 4 °C warming levels under the SSP1-2.6 scenario. Under the SSP2-4.5 scenario with an intermediate forcing level, all 18 models reached the 2 °C warming level, with the earliest and latest warming target years in 2033 and 2071, respectively; 6 models reached the 3 °C warming level, and the earliest warming target year was 2061, while the latest was 2085; there was no model that reached the 4 °C warming level.

Under the SSP5-8.5 scenario with high radiative forcing, all 18 models reached 2 and 3 °C warming levels with target year ranges of 2029-2049 and 2045-2075, respectively; 11 models reached the 4 °C warming level with a target year range of 2059-2080. Overall, there were 45, 24, and 11 datasets for the 2, 3, and 4 °C warming scenarios, respectively.

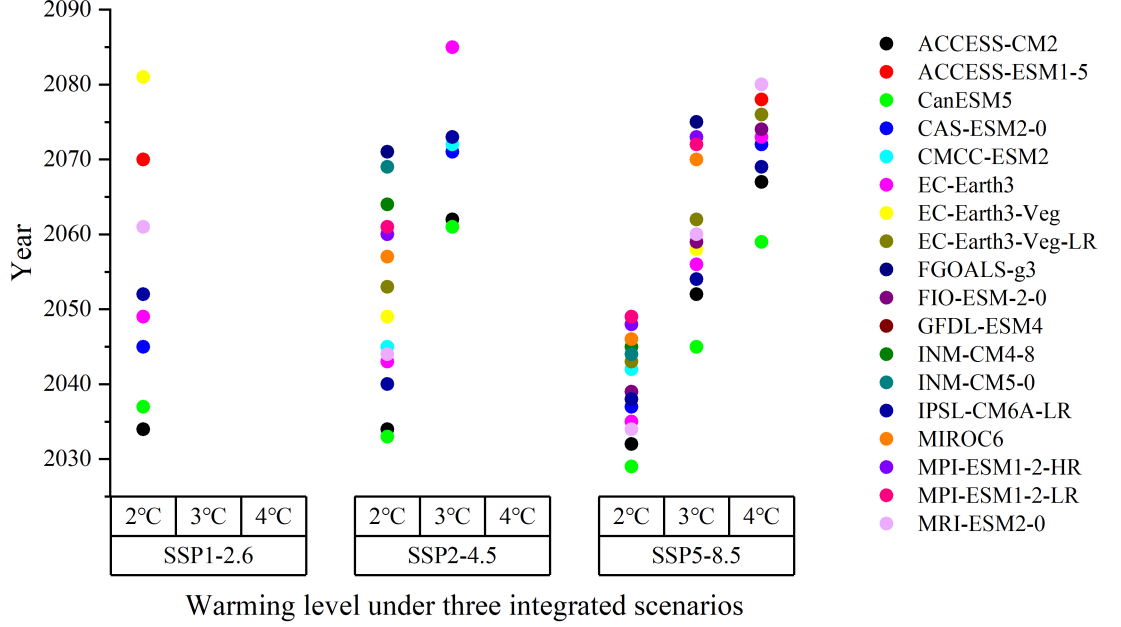


Figure 3. The warming target year of each model under 3 integrated scenarios.

4.3 Spatial Distribution and Variation in Drought Characteristics

The spatial distribution of drought frequency during the four periods is shown in Figure 4. Overall, the drought frequency in the eastern monsoon region of China showed a spatial pattern of high in the south and low in the north. The drought frequency in region G was relatively low during all periods, while the drought frequency in region F had different characteristics for different periods. During the historical reference period, the drought frequency was highest in region C, followed by the southern part of region F. Under the 2 °C warming scenario, the drought frequency across the country increased overall relative to the historical reference period, and its spatial distribution was similar to that of the historical reference period. Under the 3 °C warming scenario, the drought frequency continued to increase in most regions relative to the 2 °C warming scenario, while it decreased in region F. Droughts occurred more frequently in eastern China under the 4 °C warming scenario compared to the 3 °C warming

scenario, while drought frequency decreased significantly in regions F and G. The minimum value of drought frequency for all periods was 1.35 times/year, and the maximum value was 2.22 times/year.

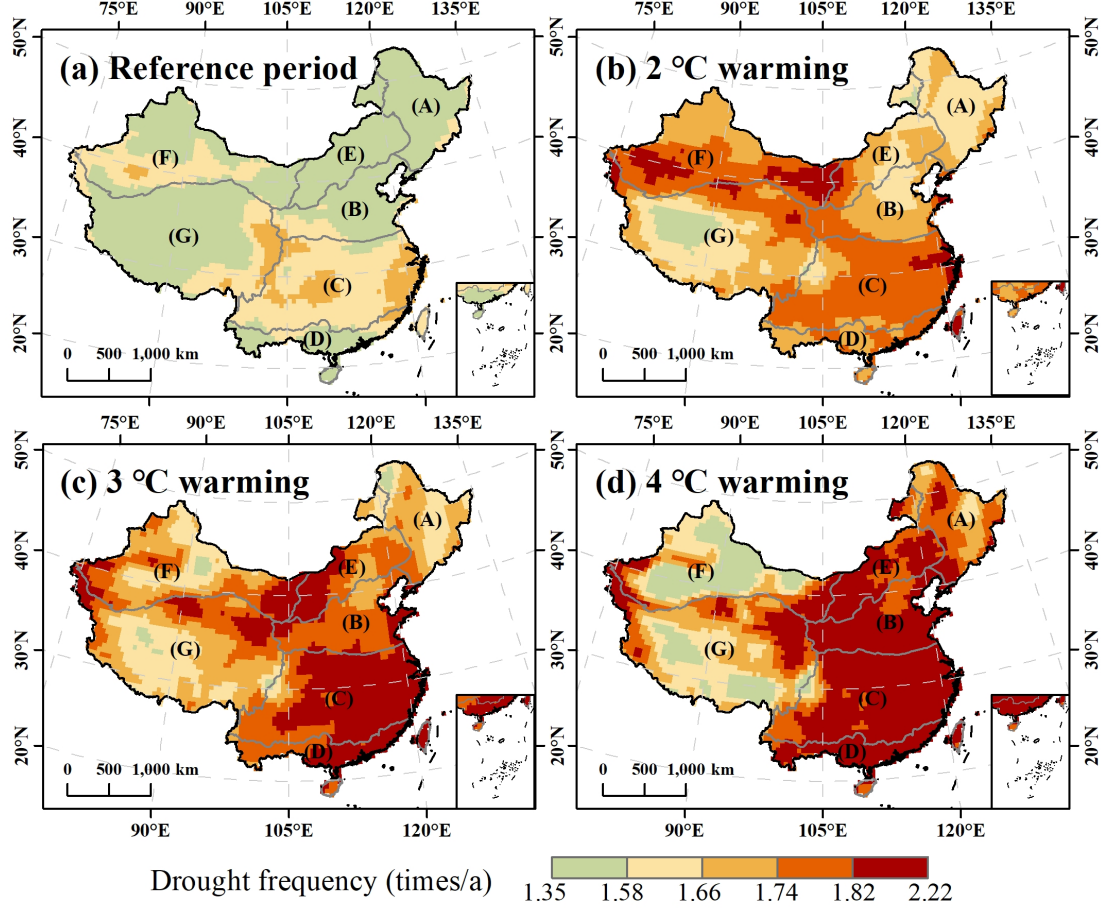


Figure 4. Spatial distribution of drought frequency under the historical reference period and three warming scenarios.

The high value of drought frequency represents the frequent occurrence of drought events, resulting in the corresponding areas being frequently hit by drought. However, a low value of drought frequency does not necessarily mean a less severe impact because a low frequency may be associated with drought events with long duration and great impact. Therefore, we further analyzed drought duration, intensity, and peak, and their spatial distribution is shown in Figure 5. Overall, three characteristics generally showed a spatial pattern of high in the northwest and low in the southeast, and the values of the characteristics increased as a whole with the increase in the warming level.

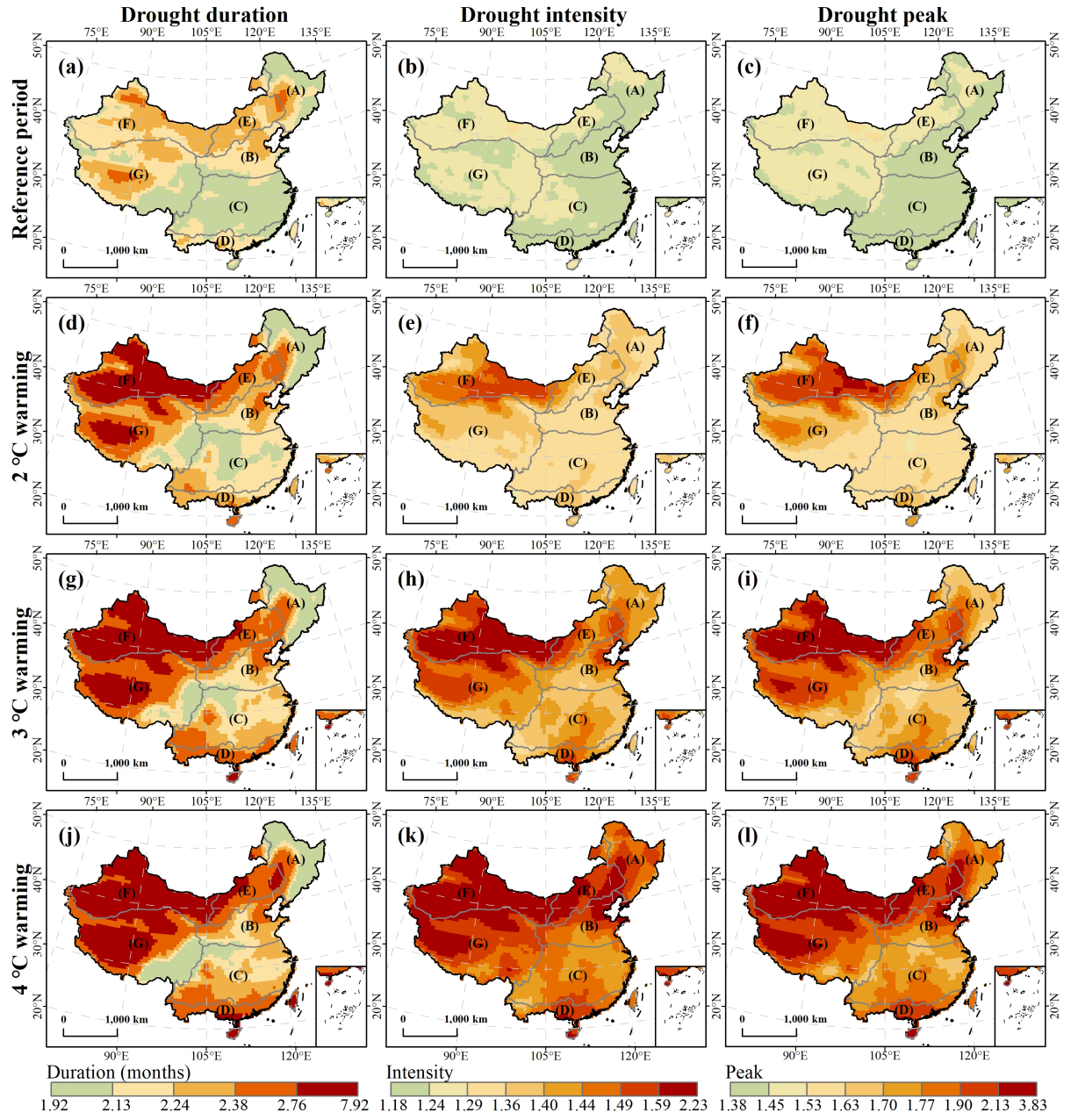


Figure 5. Spatial distribution of drought duration, intensity, and peak under the historical reference period and three warming scenarios.

The spatial distribution of drought duration is shown in Figure 5(a, d, g, j),

with longer drought durations in region F, the western Qinghai-Tibet Plateau, region E, southwestern region A, northern region B, and southwestern China. During the historical reference period, the drought duration did not exceed 2.13 months in most areas of southern China, while most areas in northern and northwestern China exceeded 2.24 months. With the increase in warming level, the drought duration increased in all regions of the country as a whole, but there was no significant increase in the northeastern edge of China and the southeastern Qinghai-Tibet Plateau. Under the 3 and 4 °C warming scenarios, drought events in northwestern China and the western Qinghai-Tibet Plateau had longer drought durations, which were associated with the lower drought frequency in the corresponding regions in Figure 4(c, d).

The spatial distribution of the drought intensity and peak is shown in Figure 5(b, e, h, k) and Figure 5(c, f, i, l), and the spatial patterns of the two characteristics were highly similar. During the historical reference period, the drought intensity basically did not exceed 1.29, and the drought peak basically did not exceed 1.53. With the increase in the warming level, the drought intensity and peak increased rapidly overall throughout the country. Under the 4 °C warming scenario, the maximum values of the drought intensity and peak reached 2.23 and 3.83, respectively, with significant increases relative to the values of the historical reference period.

4.4 Analysis of Drought Hazard Index

The drought hazard grades were recorded as I, II, III, IV, V, VI, VII, and VIII in ascending order, and the corresponding DHI ranges were 0.162~0.185, 0.185~0.202, 0.202~0.231, 0.231~0.249, 0.249~0.270, 0.270~0.292, 0.292~0.341, and 0.341~0.515, respectively. The spatial distribution of drought hazard grades during the four periods is shown in Figure 6. Overall, the drought hazard showed a spatial pattern of relatively high in the northwestern interior and southeastern coastal areas. With the increase in the warming level, the drought hazard as a whole continued to increase, and the increase was obvious in region F, northeastern region E, and the southeastern coast of China. In contrast, the drought hazard grade in the southeastern Qinghai-Tibet Plateau decreased under the 3 °C warming scenario compared with the 4 °C warming scenario.

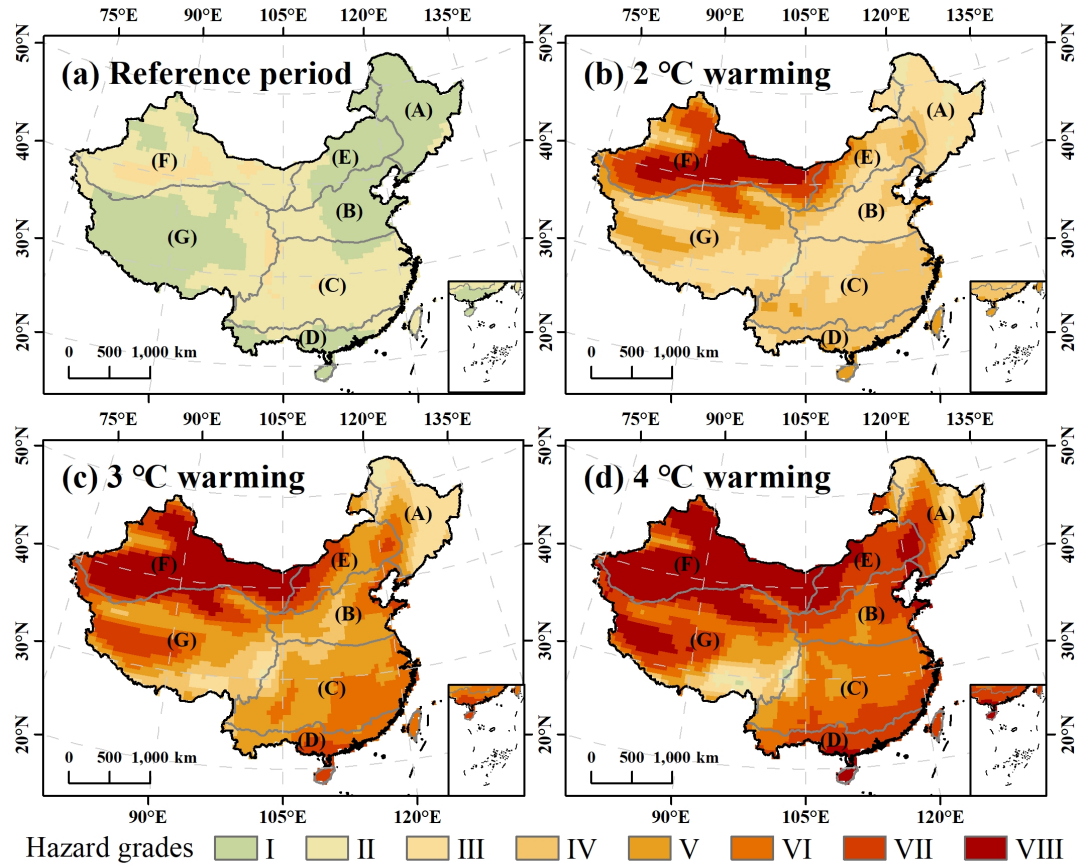


Figure 6. Spatial distribution of drought hazard grades under the historical reference period and three warming scenarios.

The proportion of grids of each drought hazard grade during the four periods was counted, as shown in Figure 7. In the historical reference period, the grades of most grids were I and II, and only approximately 4% of the grids reached grade III, while the grade reached VIII under the three warming scenarios. The grades that accounted for more than 20% were III and IV under the 2 °C warming scenario. The proportion of grades V and VI exceeded 20% under the 3 °C warming scenario, while grades VI, VII and VIII accounted for more than 20% under the 4 °C warming scenario. With the increase in warming level, the proportion of grades II, III and IV decreased, while the proportion of grades VI, VII and VIII increased.

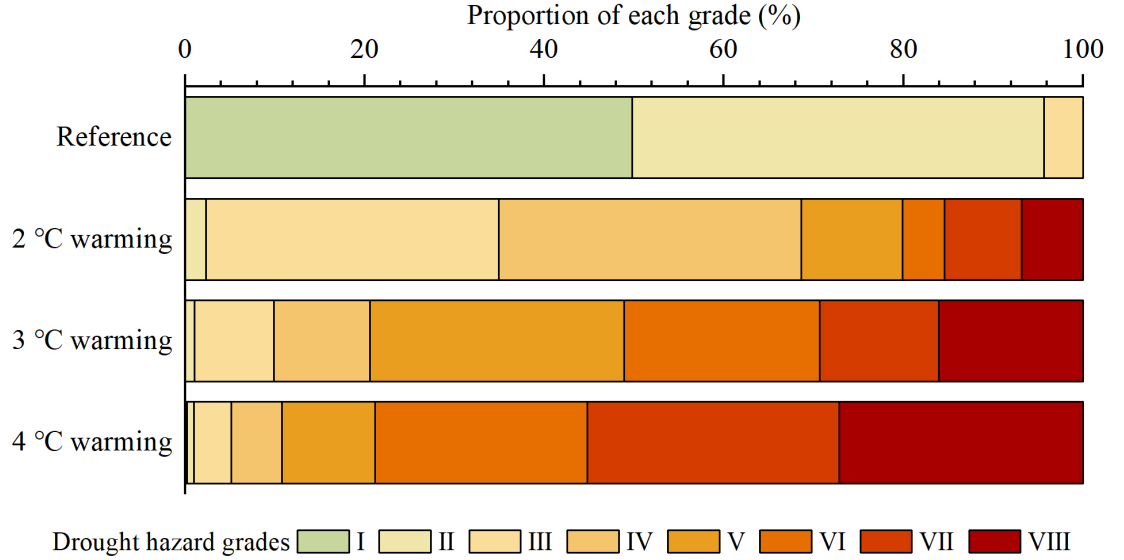


Figure 7. Statistical chart of drought risk grades under the historical reference period and three warming scenarios.

We further plotted the box plot of the DHI for the whole country and its seven climate regions for four periods, as shown in Figure 8. The maximum, median, and mean values had the same trend nationwide, increasing sequentially from the historical reference period to the 4 °C warming scenario. The mean values of the national DHI for the four periods were 0.18, 0.25, 0.29, and 0.32. The largest increase in the national DHI between two adjacent periods occurred between the historical reference period and the 2 °C warming scenario, which indicated that global warming of 2 °C and above may cause a significant increase in drought hazard in China compared with the past. The values of national DHI in the historical reference period ranged from 0.16 to 0.21, with the smallest range and the mean value approximately equal to the median. Under the three warming scenarios, the range increased in turn, and the nationwide mean values were all greater than the median. In terms of regional DHI, in the historical reference period, the maximum value of the DHI appeared in region F; the median of the DHI ranked basically in the same order as the mean value, from high to low: region F > C > D > G > B > E > A. Under the three warming scenarios, the maximum value of the DHI still occurred in region F; the three regions with the highest mean values of the DHI were regions F, E, and D, while the region with the lowest mean value was region A. Overall, the maximum, median, and mean values of the DHI in the seven climate regions increased with increasing warming level.

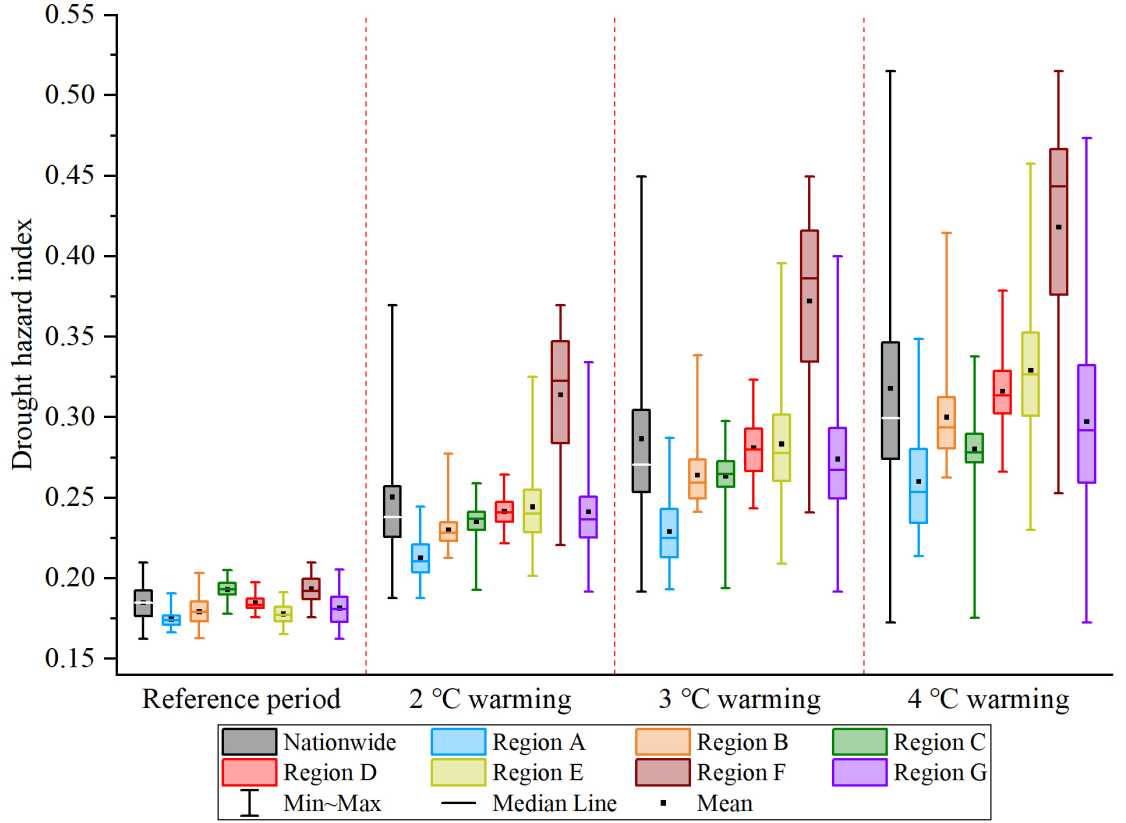


Figure 8. Box plot of DHI for the whole country and seven climate regions under the historical reference period and three warming scenarios.

4.5 Analysis of Change in Drought Hazard Index

The DHI values of the three warming scenarios minus the DHI values of the historical reference period are used to analyze the changes in drought hazard in China under different warming scenarios relative to the historical reference period (Figure 9). The DHI increased in all regions of the country except for the southeastern part of the Qinghai-Tibet Plateau, where the DHI decreased slightly. Under the three warming scenarios, the DHI increased most significantly in region F, and the increases in region E, the northeastern part of region B, the western part of the Qinghai-Tibet Plateau, and region D were also significant, while the increase in region C was relatively small. Comparing the three warming scenarios, it can be seen that the change value of DHI increased with the increase in warming level overall, but the area where the DHI decreased under the 4 °C warming scenario was slightly expanded in the southeastern part of the Qinghai-Tibet Plateau.

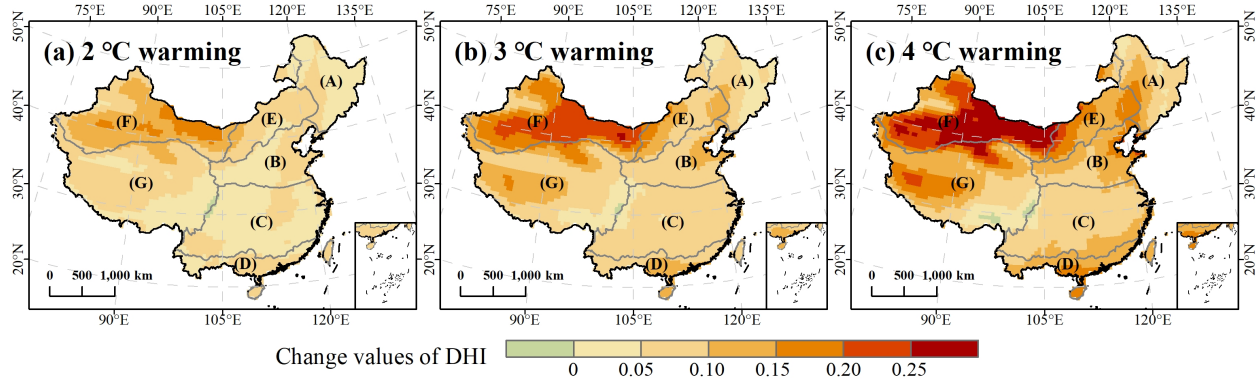


Figure 9. Spatial distribution of change values of DHI (the DHI values in the future minus DHI values in the reference period) under three warming scenarios.

Figure 10 shows the box plots of DHI change values in the whole country and seven climate regions under three warming scenarios. The national mean change values of the DHI were 0.066, 0.102, and 0.133 for the 2, 3, and 4 °C warming scenarios, respectively, and the national average increase values of DHI at 3 °C and 4 °C warming levels reached 1.5 times and 2 times that at 2 °C warming level. The national maximum, median, mean and range of the change values were the smallest under the 2 °C warming scenario and the largest under the 4 °C warming scenario. Combined with Figure 9 and Figure 10, we find that (1) the regional mean, median, and maximum values of the variation values were all positive, and only the minimum values of region C and the Qinghai-Tibet Plateau were negative, indicating that the grids with decreasing DHI only appeared in these two regions. (2) In terms of the regional means of the change values, the increase values of regions F and E were the largest and were greater than the national average, while the values of the other five regions were smaller than the national average, and the smallest increase value was in region A, followed by region C. (3) Comparing the three warming scenarios, the mean, median, and maximum values of the change in each region increased with increasing warming level.

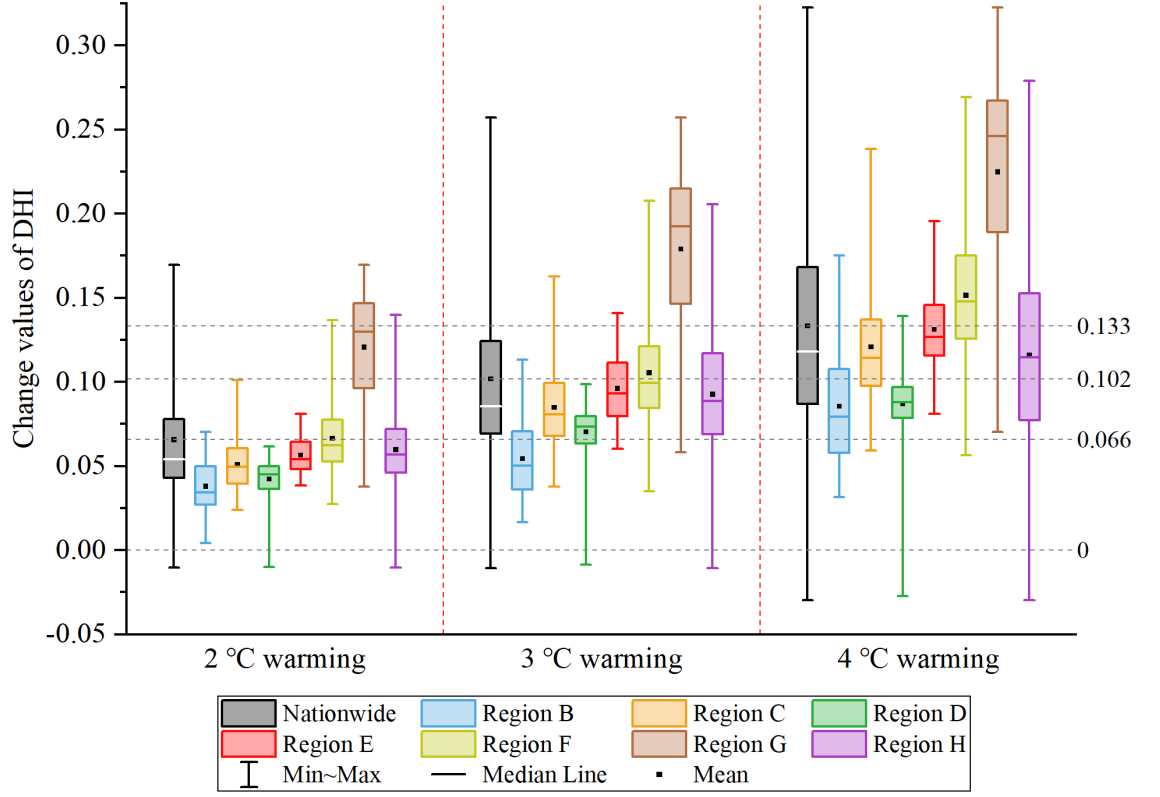


Figure 10. Box plot of change values of DHI for the whole country and seven climate regions under three warming scenarios.

5 Discussion

In this study, the DHI was constructed based on four drought characteristics, namely, drought frequency, drought duration, drought intensity, and drought peak, which can effectively integrate multiple characteristics of drought events and thus comprehensively assess drought hazards. Previous studies used different data and drought indices, as well as different methods, to construct the composite drought hazard index; therefore, the spatial and temporal patterns of drought hazard may differ from the results of this study in detail. However, the spatial and temporal characteristics of the drought from our study were generally consistent with the results of previous studies. For example, based on CMIP5 climate model data, Yao et al. (2020) predicted that drought would become more frequent and severe across most of China in the future, and drought frequency would decrease while drought severity would increase in northwestern China. The results obtained by Su et al. (2021) using CMIP6 data showed that

drought events in humid and semihumid regions of China would become more frequent in the late 21st century, while drought events in arid and semiarid regions were characterized by longer durations throughout the 21st century, and drought intensity in the future would increase in almost all regions of China, especially in northwest China. Ma et al. (2022) assessed the spatial and temporal patterns of drought in China based on CMIP6 data and found that China would experience longer duration and higher intensity droughts in the future under high emission scenarios. Gong et al. (2021) calculated the drought hazard index integrating four subindicators that reflected drought duration, intensity and frequency based on CMIP5 climate model data and predicted a significantly increasing trend of drought in central and western China, especially in northern Xinjiang Province, northwestern Gansu Province, and western Inner Mongolia, which was basically consistent with our findings. Although previous studies were conducted based on different climate scenarios without focusing on specific warming levels, they all predicted the spatial distribution and change in future drought characteristics in China, and the results were similar to those of this study.

Although it has been suggested that precipitation in China will increase in the future (Chen & Frauenfeld, 2014; Tian et al., 2021), which may ease drought, the results of our study suggest that drought hazards in China will become more severe overall in the future under global warming. Drought is influenced by the mean and variability of precipitation (Ukkola et al., 2020), and an increase in the mean value of precipitation does not necessarily lead to a decrease in drought hazard. However, global warming leads to an increase in evapotranspiration, thus causing an increase in drought to some extent. In this study, the drought hazard in the southeastern Qinghai-Tibet Plateau did not increase with the increase in warming level, which suggested that the mechanism of drought change of the Qinghai-Tibet Plateau in the context of global warming may be quite different from that of other regions. Previous studies have shown that the Qinghai-Tibet Plateau surface has experienced rapid warming and wetting as a whole in recent years, which was related to differential heating of the elevated region and its surroundings, as well as changes in local atmospheric circulations (Gao et al., 2014; Yang et al., 2014). In addition, the melting of the cryosphere might play an important role in drought variation by changing latent heat, surface albedo and other variables that influence evapotranspiration (Gao et al., 2015; Li et al., 2019). However, some studies suggest that climate model data may underestimate the temperature and overestimate the precipitation in the eastern Qinghai-Tibet Plateau (Lun et al., 2021; Su et al., 2013), so the reasons for the change in future drought hazards in the Qinghai-Tibet Plateau need to be further explored.

Drought risk depends not only on the hazard of drought but also on the number and value of disaster-bearing bodies exposed to drought and their own vulnerability characteristics. The mean values of population and GDP from 2015 to 2100 for the three SSPs (SSP1, SSP2 and SSP5) are shown in Figure 11. The population and GDP projections with a spatial resolution of $0.5^{\circ} \times 0.5^{\circ}$ under

different SSPs are available at <https://doi.org/10.57760/sciencedb.01683>. The dense population and high GDP in the eastern monsoon region of China result in a large population and assets exposed to drought hazards, and thus, the increase in drought hazard may have a great socioeconomic impact. Among the hotspots with significantly increased drought hazard in eastern China, the southern part of region A and the northern part of region B are the main production areas of corn, peanuts and other crops, and the southeast coastal area of China is the main production area of rice, so strengthening drought prevention and control in these areas is of great significance to ensure food security in China. The population and GDP of northwest China are relatively small under the three SSPs, which may result in relatively less socioeconomic risk to drought compared with eastern China. However, as we predict a noticeable increase in drought hazard in northwest China, more attention should also be paid to drought prevention in this region in the future.

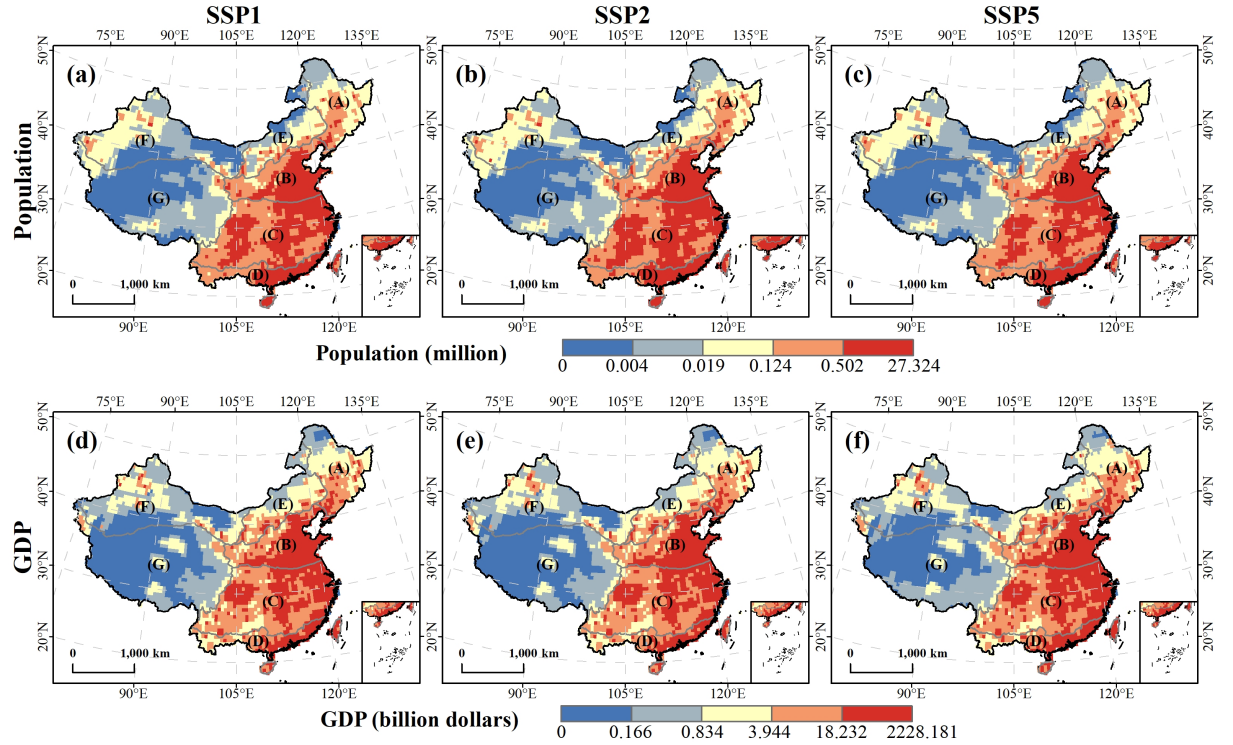


Figure 11. Population and GDP projections in China averaged from 2015 to 2100 under three SSPs.

Finally, our research also had some uncertainties and limitations. First, in terms of CMIP6 data selection, three commonly used climate scenarios, SSP1-2.6, SSP2-4.5, and SSP5-8.5, were selected in this study, while only three climate scenarios may not be representative enough due to the uncertainty of future cli-

mate change, so more climate scenarios can be included in further studies to provide more comprehensive reference information for future drought management. Second, this study used the raw climate model outputs without bias correction because bias correction does not correct the deficiencies of model simulations in representing fundamental physical processes (Ayugi et al., 2021; Ehret et al., 2012). In addition, the computation of the SPEI can act as an indirect bias correction of all the relevant variables because the SPEI values are standardized and drought events were identified using dimensionless thresholds corresponding to specific probability values (Naumann et al., 2018). Third, the SPEI drought index was used in this study, but it was reported that the PET (potential evapotranspiration)-based drought indices may overestimate the severity of drought under climate warming because the PET may be much higher than the evapotranspiration and precipitation in nonhumid regions (G. Zhang et al., 2021). It is recommended to work with multiple drought indices when assessing drought because the use of a single index may not represent all aspects of the drought situation correctly (Bank, 2019). Therefore, it is necessary to combine a number of drought indices to provide more insight into drought hazards. Fourth, the normalization method to calculate DHI used in this study was the maximum-minimum method, and the DHI for history and future ranged from 0.16 to 0.52. Considering that there may be outliers in the data, we tried to replace the minimum and maximum values with the 1st and 99th percentiles for normalization, respectively, and the new DHI ranged from 0.12 to 0.89. The range of the new DHI increased evidently relative to the original result, indicating that replacing the extremums with percentiles can exclude the influence of outliers to a certain extent. The new result of DHI was further divided into eight hazard grades using the quantile method, and we found that the spatial distribution of the new result (Figure 12) was basically the same as the original result (Figure 6), which proved that the selection of the extremums for normalization did not have an obvious effect on the spatial and temporal pattern of the DHI.

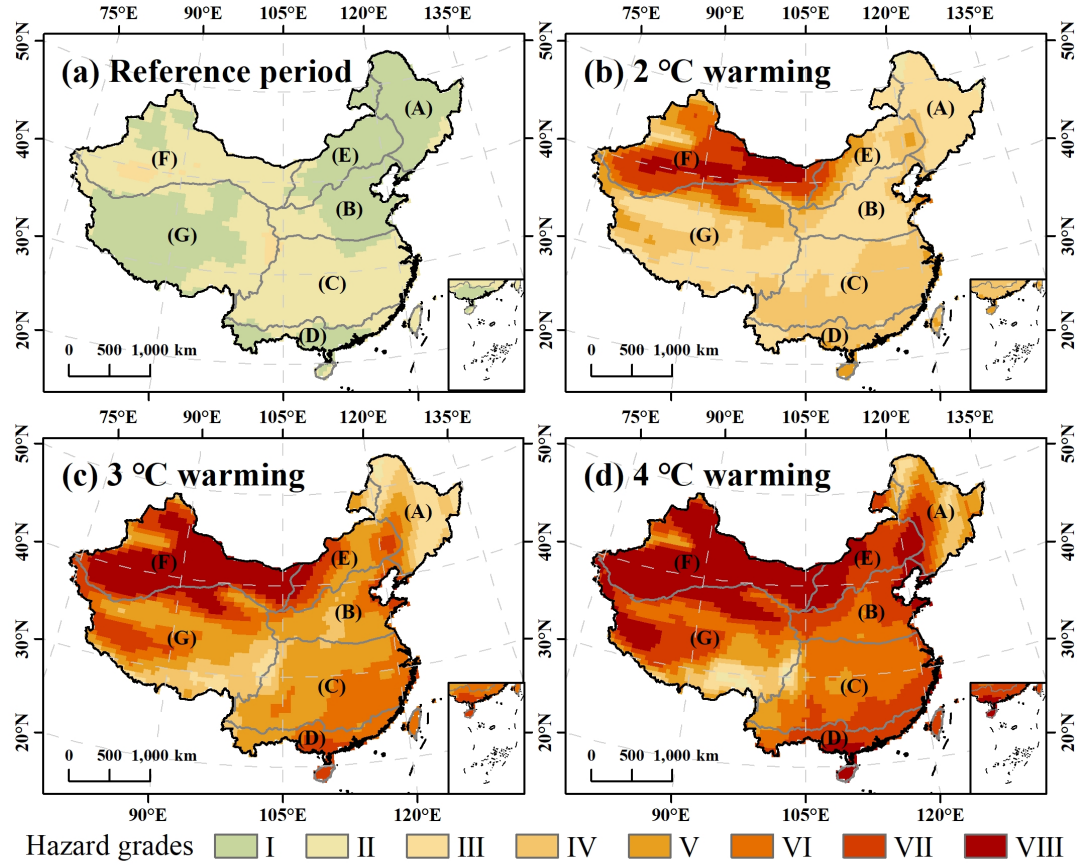


Figure 12. Spatial distribution of drought hazard grades after replacing the extremums with percentiles for normalization.

6 Conclusions

Using the data of 18 climate models of CMIP6, this paper determines the time when each model reaches the temperature rise level of 2, 3 and 4 °C, calculates the SPEI and four drought characteristic indicators, namely, drought frequency, duration, intensity and peak, under the historical reference period and three future temperature rise scenarios, and then constructs the drought hazard index (DHI). The DHI of the historical reference period and the future 2, 3 and 4 °C temperature rise scenarios were evaluated and compared. The main conclusions are as follows:

- (1) The four drought characteristic indicators have obvious spatial differentiation. The drought frequency in the eastern monsoon region of China showed a

spatial distribution of high in the south and low in the north, and the drought frequency increases as the temperature rises. The drought frequency of the Qinghai-Tibet Plateau and the northwest desert region first increased and then decreased with increasing temperature. The drought duration, intensity and peak at each period showed a spatial distribution of high in northwest China and low in southeast China. The characteristic indicator values increased significantly with increasing temperature.

(2) The DHI values in the northwest inland and southeast coastal areas of China were higher, which corresponds to the larger drought duration, intensity and peak values in the northwest inland areas and the larger drought frequency in the southeast coastal areas. The largest regional mean of DHI was in the northwest desert area, and the smallest was in the northeast humid and semihumid temperate region. With the increase in temperature rise, the DHI in the whole country and the seven climate regions was increasing, but the drought hazard level in the southeast of the Qinghai-Tibet Plateau was significantly reduced from 3 °C to 4 °C.

(3) Compared with the historical reference period, the DHI under the scenarios of 2, 3 and 4 °C temperature increases in the future primarily increased in all climate regions of China, except southeast of the Qinghai-Tibet Plateau. The increase in DHI in the northwest desert area is the most obvious. Overall, the change in the DHI relative to the historical reference period increases with increasing temperature. The national average values of the increase in DHI under the 3 °C and 4 °C temperature rise scenarios reached 1.5 times and 2 times that under the 2 °C temperature rise scenario, respectively.

Acknowledgments

This work was supported by the National Key R&D Program of China (Grant No. 2019YFA0606900) and the National Natural Science Foundation of China (Grant No. 42077436). We thank the Institute of Atmospheric Physics, Chinese Academy of Sciences, for providing the CN05.1 dataset. The authors declare no conflicts of interests.

Data and Software Availability Statement

The CMIP6 simulations are available from <https://esgf-node.llnl.gov/search/cmip6/>.

The GMTED2010 dataset can be accessed from <https://earthexplorer.usgs.gov/>.

The population and GDP projections under different SSPs can be accessed from <https://doi.org/10.57760/sciencedb.01683>.

The version 1.7 of the SPEI R library used for the calculation of the SPEI is available from <https://cran.r-project.org/web/packages/SPEI/index.html>.

References

- Ayantobo, O. O., Li, Y., Song, S., Javed, T., & Yao, N. (2018). Probabilistic modelling of drought events in China via 2-dimensional joint copula. *JOURNAL OF HYDROLOGY*, 559, 373-391. <http://doi.org/https://doi.org/10.1016/j.jhydrol.2018.02.022>
- Ayugi, B., Dike, V., Ngoma, H., Babaousmail, H., Mumo, R., & Ongoma, V. (2021). Future Changes in Precipitation Extremes over East Africa Based on CMIP6 Models. *Water (Basel)*, 13(17), 2358. <http://doi.org/10.3390/w13172358>
- Babaousmail, H., Ayugi, B., Rajasekar, A., Zhu, H., Oduro, C., Mumo, R., & Ongoma, V. (2022). Projection of Extreme Temperature Events over the Mediterranean and Sahara Using Bias-Corrected CMIP6 Models. *Atmosphere*, 13(5), 741. <http://doi.org/10.3390/atmos13050741>
- Bank, W. (2019). *Assessing Drought Hazard and Risk : Principles and Implementation Guidance*. Washington, DC: World Bank.
- Beguería, S., Vicente-Serrano, S. M., Reig, F., & Latorre, B. (2014). Standardized precipitation evapotranspiration index (SPEI) revisited: parameter fitting, evapotranspiration models, tools, datasets and drought monitoring. *INTERNATIONAL JOURNAL OF CLIMATOLOGY*, 34(10), 3001-3023. <http://doi.org/https://doi.org/10.1002/joc.3887>
- Chen, H., Sun, J., Lin, W., & Xu, H. (2020). Comparison of CMIP6 and CMIP5 models in simulating climate extremes. *Science Bulletin*, 65(17), 1415-1418. <http://doi.org/https://doi.org/10.1016/j.scib.2020.05.015>
- Chen, L., Wang, G., Miao, L., Gnyawali, K. R., Li, S., Amankwah, S. O. Y., Huang, J., Lu, J., & Zhan, M. (2021). Future drought in CMIP6 projections and the socioeconomic impacts in China. *INTERNATIONAL JOURNAL OF CLIMATOLOGY*, 41(8), 4151-4170. <http://doi.org/https://doi.org/10.1002/joc.7064>
- Chen, L., & Frauenfeld, O. W. (2014). A comprehensive evaluation of precipitation simulations over China based on CMIP5 multimodel ensemble projections. *Journal of Geophysical Research: Atmospheres*, 119(10), 5767-5786. <http://doi.org/https://doi.org/10.1002/2013JD021190>
- Cook, B. I., Mankin, J. S., Marvel, K., Williams, A. P., Smerdon, J. E., & Anchukaitis, K. J. (2020). Twenty-First Century Drought Projections in the CMIP6 Forcing Scenarios. *Earth's Future*, 8(6), e1461E-e2019E. <http://doi.org/https://doi.org/10.1029/2019EF001461>
- Danielson, J. J., & Gesch, D. B. (2011). *Global multi-resolution terrain elevation data 2010 (GMTED2010)*. Washington, DC: US Department of the Interior, US Geological Survey.

- Dike, V. N., Lin, Z., Fei, K., Langendijk, G. S., & Nath, D. (2022). Evaluation and multimodel projection of seasonal precipitation extremes over central Asia based on CMIP6 simulations. *INTERNATIONAL JOURNAL OF CLIMATOLOGY*, n/a(n/a). <http://doi.org/https://doi.org/10.1002/joc.7641>
- Ehret, U., Zehe, E., Wulfmeyer, V., Warrach-Sagi, K., & Liebert, J. (2012). HESS Opinions "Should we apply bias correction to global and regional climate model data?". *Hydrol. Earth Syst. Sci.*, 16(9), 3391-3404. <http://doi.org/10.5194/hess-16-3391-2012>
- Eyring, V., Bony, S., Meehl, G. A., Senior, C. A., Stevens, B., Stouffer, R. J., & Taylor, K. E. (2016). Overview of the Coupled Model Intercomparison Project Phase 6 (CMIP6) experimental design and organization. *Geoscientific Model Development*, 9(5), 1937-1958. <http://doi.org/10.5194/gmd-9-1937-2016>
- Fan, X., Miao, C., Duan, Q., Shen, C., & Wu, Y. (2020). The Performance of CMIP6 Versus CMIP5 in Simulating Temperature Extremes Over the Global Land Surface. *Journal of Geophysical Research: Atmospheres*, 125(18), e2020Je33031J. <http://doi.org/https://doi.org/10.1029/2020JD033031>
- Gao, Y., Cuo, L., & Zhang, Y. (2014). Changes in Moisture Flux over the Tibetan Plateau during 1979–2011 and Possible Mechanisms. *JOURNAL OF CLIMATE*, 27(5), 1876-1893. <http://doi.org/10.1175/JCLI-D-13-00321.1>
- Gao, Y., Li, X., Ruby Leung, L., Chen, D., & Xu, J. (2015). Aridity changes in the Tibetan Plateau in a warming climate. *Environmental Research Letters*, 10(3), 34013. <http://doi.org/10.1088/1748-9326/10/3/034013>
- Geng, G., Wu, J., Wang, Q., Lei, T., He, B., Li, X., Mo, X., Luo, H., Zhou, H., & Liu, D. (2016). Agricultural drought hazard analysis during 1980–2008: a global perspective. *INTERNATIONAL JOURNAL OF CLIMATOLOGY*, 36(1), 389-399. <http://doi.org/https://doi.org/10.1002/joc.4356>
- Gong, X., Du, S., Li, F., & Ding, Y. (2021). Study on the Spatial and Temporal Characteristics of Mesoscale Drought in China under Future Climate Change Scenarios. *Water (Basel)*, 13(19), 2761. <http://doi.org/10.3390/w13192761>
- Hayes, M. J., Wilhelmi, O. V., & Knutson, C. L. (2004). Reducing Drought Risk: Bridging Theory and Practice. *Natural Hazards Review*, 5(2), 106-113. [http://doi.org/10.1061/\(ASCE\)1527-6988\(2004\)5:2\(106\)](http://doi.org/10.1061/(ASCE)1527-6988(2004)5:2(106))
- He, B., Lü, A., Wu, J., Zhao, L., & Liu, M. (2011). Drought hazard assessment and spatial characteristics analysis in China. *Journal of Geographical Sciences*, 21(2), 235-249. <http://doi.org/10.1007/s11442-011-0841-x>
- IPCC. (2014). *Climate Change 2013 – The Physical Science Basis: Working Group I Contribution to the Fifth Assessment Report of the Intergovernmental Panel on Climate Change*. Cambridge: Cambridge University Press. <https://doi.org/DOI: 10.1017/CBO9781107415324>

- IPCC. (2021). *Climate Change 2021: The Physical Science Basis. Contribution of Working Group I to the Sixth Assessment Report of the Intergovernmental Panel on Climate Change* (Vol. In Press). Cambridge, United Kingdom and New York, NY, USA: Cambridge University Press. <https://doi.org/10.1017/9781009157896>
- IPCC. (2022a). *Climate change 2022: Impacts, Adaptation and Vulnerability. Contribution of Working Group II to the Sixth Assessment Report of the Intergovernmental Panel on Climate Change* (Vol. In Press). Cambridge, United Kingdom and New York, NY, USA: Cambridge University Press.
- IPCC. (2022b). *Global Warming of 1.5°C: IPCC Special Report on Impacts of Global Warming of 1.5°C above Pre-industrial Levels in Context of Strengthening Response to Climate Change, Sustainable Development, and Efforts to Eradicate Poverty*. Cambridge: Cambridge University Press. <https://doi.org/DOI:10.1017/9781009157940>
- James, R., Washington, R., Schleussner, C., Rogelj, J., & Conway, D. (2017). Characterizing half-a-degree difference: a review of methods for identifying regional climate responses to global warming targets. *WIREs Climate Change*, 8(2), e457. <http://doi.org/https://doi.org/10.1002/wcc.457>
- Jiao, Y., & Yuan, X. (2019). More severe hydrological drought events emerge at different warming levels over the Wudinghe watershed in northern China. *HYDROLOGY AND EARTH SYSTEM SCIENCES*, 23(1), 621-635. <http://doi.org/10.5194/hess-23-621-2019>
- Kuang, X., Huang, D., & Huang, Y. (2021). Inconsistent variation of return periods of temperature extremum in China and its projection based on CMIP6 results. *SN Applied Sciences*, 3(12), 868. <http://doi.org/10.1007/s42452-021-04863-3>
- Li, H., Li, Z., Chen, Y., Liu, Y., Hu, Y., Sun, F., & Kayumba, P. (2021). Projected Meteorological Drought over Asian Drylands under Different CMIP6 Scenarios. *Remote sensing (Basel, Switzerland)*, 13(21), 4409. <http://doi.org/10.3390/rs13214409>
- Li, H., Liu, L., Shan, B., Xu, Z., Niu, Q., Cheng, L., Liu, X., & Xu, Z. (2019). Spatiotemporal Variation of Drought and Associated Multi-Scale Response to Climate Change over the Yarlung Zangbo River Basin of Qinghai-Tibet Plateau, China. *Remote sensing (Basel, Switzerland)*, 11(13), 1596. <http://doi.org/10.3390/rs11131596>
- Li, L., She, D., Zheng, H., Lin, P., & Yang, Z. (2020). Elucidating Diverse Drought Characteristics from Two Meteorological Drought Indices (SPI and SPEI) in China. *JOURNAL OF HYDROMETEOROLOGY*, 21(7), 1513-1530. <http://doi.org/10.1175/JHM-D-19-0290.1>
- Liu, Y., Chen, J., & Pan, T. (2021). Spatial and temporal patterns of drought hazard for China under different RCP scenarios in the 21st

- century. *International Journal of Disaster Risk Reduction*, 52, 101948. <http://doi.org/https://doi.org/10.1016/j.ijdrr.2020.101948>
- Liu, Y., Geng, X., Hao, Z., & Zheng, J. (2020). Changes in Climate Extremes in Central Asia under 1.5 and 2 °C Global Warming and their Impacts on Agricultural Productions. *Atmosphere*, 11(10), 1076. <http://doi.org/10.3390/atmos11101076>
- Lun, Y., Liu, L., Cheng, L., Li, X., Li, H., & Xu, Z. (2021). Assessment of GCMs simulation performance for precipitation and temperature from CMIP5 to CMIP6 over the Tibetan Plateau. *INTERNATIONAL JOURNAL OF CLIMATOLOGY*, 41(7), 3994-4018. <http://doi.org/https://doi.org/10.1002/joc.7055>
- Luo, N., Guo, Y., Gao, Z., Chen, K., & Chou, J. (2020). Assessment of CMIP6 and CMIP5 model performance for extreme temperature in China. *Atmospheric and oceanic science letters = Daqi-he-haiyang-ke-xue-kuaibao*, 13(6), 589-597. <http://doi.org/10.1080/16742834.2020.1808430>
- Ma, Z., Sun, P., Zhang, Q., Zou, Y., Lv, Y., Li, H., & Chen, D. (2022). The Characteristics and Evaluation of Future Droughts across China through the CMIP6 Multi-Model Ensemble. *Remote sensing (Basel, Switzerland)*, 14(1097), 1097. <http://doi.org/10.3390/rs14051097>
- Maccioni, P., Kossida, M., Brocca, L., & Moramarco, T. (2015). Assessment of the Drought Hazard in the Tiber River Basin in Central Italy and a Comparison of New and Commonly Used Meteorological Indicators. *JOURNAL OF HYDROLOGIC ENGINEERING*, 20(8), 5014029. [http://doi.org/10.1061/\(ASCE\)HE.1943-5584.0001094](http://doi.org/10.1061/(ASCE)HE.1943-5584.0001094)
- McKee, T. B., Doesken, N. J., & Kleist, J. (1993). *The relationship of drought frequency and duration to time scales*. Paper presented at the Proceedings of the 8th Conference on Applied Climatology, Boston, MA.
- Miao, L., Li, S., Zhang, F., Chen, T., Shan, Y., & Zhang, Y. (2020). Future Drought in the Dry Lands of Asia Under the 1.5 and 2.0 °C Warming Scenarios. *Earth's Future*, 8(6), e1337E-e2019E. <http://doi.org/10.1029/2019EF001337>
- Mukherjee, S., Mishra, A., & Trenberth, K. E. (2018). Climate Change and Drought: a Perspective on Drought Indices. *Current Climate Change Reports*, 4(2), 145-163. <http://doi.org/10.1007/s40641-018-0098-x>
- Naderi, K., Moghaddasi, M., & Shokri, A. (2022). Drought Occurrence Probability Analysis Using Multivariate Standardized Drought Index and Copula Function Under Climate Change. *WATER RESOURCES MANAGEMENT*, 36(8), 2865-2888. <http://doi.org/10.1007/s11269-022-03186-1>
- Nam, W., Hayes, M. J., Svoboda, M. D., Tadesse, T., & Wilhite, D. A. (2015). Drought hazard assessment in the context of climate change for South Korea. *AGRICULTURAL WATER MANAGEMENT*, 160, 106-117. <http://doi.org/https://doi.org/10.1016/j.agwat.2015.06.029>

- Naumann, G., Alfieri, L., Wyser, K., Mentaschi, L., Betts, R. A., Carrao, H., Spinoni, J., Vogt, J., & Feyen, L. (2018). Global Changes in Drought Conditions Under Different Levels of Warming. *GEOPHYSICAL RESEARCH LETTERS*, 45(7), 3285-3296. <http://doi.org/https://doi.org/10.1002/2017GL076521>
- O'Neill, B. C., Tebaldi, C., van Vuuren, D. P., Eyring, V., Friedlingstein, P., Hurtt, G., Knutti, R., Kriegler, E., Lamarque, J. F., Lowe, J., Meehl, G. A., Moss, R., Riahi, K., & Sanderson, B. M. (2016). The Scenario Model Intercomparison Project (ScenarioMIP) for CMIP6. *Geoscientific Model Development*, 9(9), 3461-3482. <http://doi.org/10.5194/gmd-9-3461-2016>
- Palmer, W. C. (1965). *Meteorological drought* (Vol. 30). Washington, DC: US Department of Commerce, Weather Bureau.
- Rajulapati, C. R., Abdelmoaty, H. M., Nerantzaki, S. D., & Papalexiou, S. M. (2022). Changes in the risk of extreme temperatures in megacities worldwide. *Climate Risk Management*, 36, 100433. <http://doi.org/https://doi.org/10.1016/j.crm.2022.100433>
- Rogelj, J., den Elzen, M., Höhne, N., Fransen, T., Fekete, H., Winkler, H., Schaeffer, R., Sha, F., Riahi, K., & Meinshausen, M. (2016). Paris Agreement climate proposals need a boost to keep warming well below 2 °C. *NATURE*, 534(7609), 631-639. <http://doi.org/10.1038/nature18307>
- Shi, P., Ye, T., Wang, Y., Zhou, T., Xu, W., Du, J., Wang, J. A., Li, N., Huang, C., Liu, L., Chen, B., Su, Y., Fang, W., Wang, M., Hu, X., Wu, J., He, C., Zhang, Q., Ye, Q., Jaeger, C., & Okada, N. (2020). Disaster Risk Science: A Geographical Perspective and a Research Framework. *International Journal of Disaster Risk Science*, 11(4), 426-440. <http://doi.org/10.1007/s13753-020-00296-5>
- Singh, G. R., Jain, M. K., & Gupta, V. (2019). Spatiotemporal assessment of drought hazard, vulnerability and risk in the Krishna River basin, India. *NATURAL HAZARDS*, 99(2), 611-635. <http://doi.org/10.1007/s11069-019-03762-6>
- Spinoni, J., Barbosa, P., Bucchignani, E., Cassano, J., Cavazos, T., Christensen, J. H., Christensen, O. B., Coppola, E., Evans, J., Geyer, B., Giorgi, F., Hadjinicolaou, P., Jacob, D., Katzfey, J., Koenigk, T., Laprise, R., Lennard, C. J., Kurnaz, M. L., Li, D., Llopart, M., McCormick, N., Naumann, G., Nikulin, G., Ozturk, T., Panitz, H., Porfirio Da Rocha, R., Rockel, B., Solman, S. A., Syktus, J., Tangang, F., Teichmann, C., Vautard, R., Vogt, J. V., Winger, K., Zittis, G., & Dosio, A. (2020). Future Global Meteorological Drought Hot Spots: A Study Based on CORDEX Data. *JOURNAL OF CLIMATE*, 33(9), 3635-3661. <http://doi.org/10.1175/JCLI-D-19-0084.1>
- Su, B., Huang, J., Fischer, T., Wang, Y., Kundzewicz, Z. W., Zhai, J., Sun, H., Wang, A., Zeng, X., Wang, G., Tao, H., Gemmer, M., Li, X., & Jiang, T. (2018). Drought losses in China might double between the 1.5 °C and 2.0 °C warming. *PROCEEDINGS OF THE NATIONAL ACADEMY OF SCIENCES OF THE UNITED STATES OF AMERICA*, 115(42), 10600-10605. <http://doi.org/10.1073/pnas.1802129115>

- Su, B., Huang, J., Mondal, S. K., Zhai, J., Wang, Y., Wen, S., Gao, M., Lv, Y., Jiang, S., Jiang, T., & Li, A. (2021). Insight from CMIP6 SSP-RCP scenarios for future drought characteristics in China. *ATMOSPHERIC RESEARCH*, 250, 105375. <http://doi.org/https://doi.org/10.1016/j.atmosres.2020.105375>
- Su, F., Duan, X., Chen, D., Hao, Z., & Cuo, L. (2013). Evaluation of the Global Climate Models in the CMIP5 over the Tibetan Plateau. *JOURNAL OF CLIMATE*, 26(10), 3187-3208. <http://doi.org/10.1175/JCLI-D-12-00321.1>
- Tang, B., Hu, W., & Duan, A. (2021). Assessment of Extreme Precipitation Indices over Indochina and South China in CMIP6 Models. *JOURNAL OF CLIMATE*, 34(18), 7507-7524. <http://doi.org/10.1175/JCLI-D-20-0948.1>
- Taylor, K. E. (2001). Summarizing multiple aspects of model performance in a single diagram. *Journal of Geophysical Research: Atmospheres*, 106(D7), 7183-7192. <http://doi.org/https://doi.org/10.1029/2000JD900719>
- Tian, J., Zhang, Z., Ahmed, Z., Zhang, L., Su, B., Tao, H., & Jiang, T. (2021). Projections of precipitation over China based on CMIP6 models. *STOCHASTIC ENVIRONMENTAL RESEARCH AND RISK ASSESSMENT*, 35(4), 831-848. <http://doi.org/10.1007/s00477-020-01948-0>
- Touma, D., Ashfaq, M., Nayak, M. A., Kao, S., & Diffenbaugh, N. S. (2015). A multi-model and multi-index evaluation of drought characteristics in the 21st century. *JOURNAL OF HYDROLOGY*, 526, 196-207. <http://doi.org/https://doi.org/10.1016/j.jhydrol.2014.12.011>
- Ukkola, A. M., De Kauwe, M. G., Roderick, M. L., Abramowitz, G., & Pitman, A. J. (2020). Robust Future Changes in Meteorological Drought in CMIP6 Projections Despite Uncertainty in Precipitation. *GEOPHYSICAL RESEARCH LETTERS*, 47(11), e2020G-e87820G. <http://doi.org/https://doi.org/10.1029/2020GL087820>
- Vicente-Serrano, S. M., Beguería, S., & López-Moreno, J. I. (2010). A Multi-scalar Drought Index Sensitive to Global Warming: The Standardized Precipitation Evapotranspiration Index. *JOURNAL OF CLIMATE*, 23(7), 1696-1718. <http://doi.org/10.1175/2009JCLI2909.1>
- Wang, F., Wang, Z., Yang, H., Di, D., Zhao, Y., Liang, Q., & Hussain, Z. (2020). Comprehensive evaluation of hydrological drought and its relationships with meteorological drought in the Yellow River basin, China. *JOURNAL OF HYDROLOGY*, 584, 124751. <http://doi.org/https://doi.org/10.1016/j.jhydrol.2020.124751>
- WMO, & GWP. (2016). Handbook of Drought Indicators and Indices. In M. Svoboda & B. Fuchs (Eds.), *Integrated Drought Management Tools and Guidelines Series 2* (2021, pp.). Geneva: Integrated Drought Management Programme (IDMP).
- Wu, H., Lei, H., Lu, W., & Liu, Z. (2022). Future changes in precipitation over the upper Yangtze River basin based on bias correction spatial downscaling of models from CMIP6. *Environmental Research Communications*, 4(4), 45002. <http://doi.org/10.1088/2515-7620/ac620e>

- Wu, J., & Gao, X. J. (2013). A gridded daily observation dataset over China region and comparison with the other datasets. *Acta Geophysica Sinica*, 56(4), 1102-1111. <http://doi.org/10.6038/cjg20130406>
- Xu, H., Chen, H., & Wang, H. (2022). Future changes in precipitation extremes across China based on CMIP6 models. *INTERNATIONAL JOURNAL OF CLIMATOLOGY*, 42(1), 635-651. <http://doi.org/https://doi.org/10.1002/joc.7264>
- Yang, K., Wu, H., Qin, J., Lin, C., Tang, W., & Chen, Y. (2014). Recent climate changes over the Tibetan Plateau and their impacts on energy and water cycle: A review. *GLOBAL AND PLANETARY CHANGE*, 112, 79-91. <http://doi.org/https://doi.org/10.1016/j.gloplacha.2013.12.001>
- Yao, N., Li, L., Feng, P., Feng, H., Li Liu, D., Liu, Y., Jiang, K., Hu, X., & Li, Y. (2020). Projections of drought characteristics in China based on a standardized precipitation and evapotranspiration index and multiple GCMs. *SCIENCE OF THE TOTAL ENVIRONMENT*, 704, 135245. <http://doi.org/https://doi.org/10.1016/j.scitotenv.2019.135245>
- Yao, N., Li, Y., Lei, T., & Peng, L. (2018). Drought evolution, severity and trends in mainland China over 1961–2013. *SCIENCE OF THE TOTAL ENVIRONMENT*, 616-617, 73-89. <http://doi.org/https://doi.org/10.1016/j.scitotenv.2017.10.327>
- Yevjevich, V. M. (1967). An objective approach to definitions and investigations of continental hydrologic droughts, *Hydrol. Pap.*, vol. 23, 18 pp., Colo. State Univ., Fort Collins.
- Yihdego, Y., Vaheddoost, B., & Al-Weshah, R. A. (2019). Drought indices and indicators revisited. *Arabian Journal of Geosciences*, 12(3), 69. <http://doi.org/10.1007/s12517-019-4237-z>
- Yu, M., Li, Q., Hayes, M. J., Svoboda, M. D., & Heim, R. R. (2014). Are droughts becoming more frequent or severe in China based on the Standardized Precipitation Evapotranspiration Index: 1951–2010? *INTERNATIONAL JOURNAL OF CLIMATOLOGY*, 34(3), 545-558. <http://doi.org/https://doi.org/10.1002/joc.3701>
- Yuan, X., Zhou, Y., Jin, J., & Wei, Y. (2013). Risk analysis for drought hazard in China: a case study in Huaibei Plain. *NATURAL HAZARDS*, 67(2), 879-900. <http://doi.org/10.1007/s11069-013-0614-1>
- Zachariah, M., Mondal, A., & AghaKouchak, A. (2021). Probabilistic Assessment of Extreme Heat Stress on Indian Wheat Yields Under Climate Change. *GEOPHYSICAL RESEARCH LETTERS*, 48(20), e2021G-e94702G. <http://doi.org/https://doi.org/10.1029/2021GL094702>
- Zhang, G., Su, X., Singh, V. P., & Ayantobo, O. O. (2021). Appraising standardized moisture anomaly index (SZI) in drought projection across China under CMIP6 forcing scenarios. *Journal of Hydrology: Regional Studies*, 37, 100898. <http://doi.org/https://doi.org/10.1016/j.ejrh.2021.100898>

- Zhang, J., & Wang, F. (2019). Changes in the Risk of Extreme Climate Events over East Asia at Different Global Warming Levels. *Water (Basel)*, 11(12), 2535. <http://doi.org/10.3390/w11122535>
- Zhang, L., Chen, Z., & Zhou, T. (2021). Human Influence on the Increasing Drought Risk Over Southeast Asian Monsoon Region. *GEOPHYSICAL RESEARCH LETTERS*, 48(11), e2021G-e93777G. <http://doi.org/https://doi.org/10.1029/2021GL093777>
- Zhang, Y., Hanati, G., Danierhan, S., Liu, Q., & Xu, Z. (2020). Evaluation and Comparison of Daily GPM/TRMM Precipitation Products over the Tianshan Mountains in China. *Water (Basel)*, 12(11), 3088. <http://doi.org/10.3390/w12113088>
- Zhao, S. (1983). A new scheme for comprehensive physical regionalization in China. *Acta Geographica Sinica*, 38(1), 1-10. (In Chinese).
- Zhao, Y., Qian, C., Zhang, W., He, D., & Qi, Y. (2021). Extreme temperature indices in Eurasia in a CMIP6 multi-model ensemble: Evaluation and projection. *INTERNATIONAL JOURNAL OF CLIMATOLOGY*, 41(11), 5368-5385. <http://doi.org/https://doi.org/10.1002/joc.7134>